Channel network extraction from high resolution topography using wavelets

Bruno Lashermes,[1] Efi Foufoula-Georgiou,[1] and William E. Dietrich[2]

[1] The availability of high resolution topography from LIDAR offers new opportunities for objectively extracting the channels directly from a DEM using local topographic information, instead of inferring them indirectly based on global criteria, such as area or area-slope threshold relationships. Here we introduce the use of wavelet filtering to delineate threshold curvatures for defining valleys and threshold slope-direction-change for defining probable channeled portions of the valleys. This approach exploits the topographic signatures uniquely found in high resolution topography, and reveals the fuzzy topographic transition in which local weakly convergent areas lie at the transition between hillslopes and valleys. **Citation:** Lashermes, B., E. Foufoula-Georgiou, and W. E. Dietrich (2007), Channel network extraction from high resolution topography using wavelets, *Geophys. Res. Lett.*, *34*, L23S04, doi:10.1029/2007GL031140.

1. Introduction

[2] The automatic extraction of geomorphologic features from Digital Elevation Models (DEMs) has been a subject of considerable research over the past several decades. The two main challenges in channel network extraction algorithms from traditional DEMs have been: handling multiple direction flows [e.g., *Costa-Gabral and Burges*, 1994; *Tarboton*, 1997] and deciding where the channel begins [e.g., *Montgomery and Dietrich*, 1988, 1989, 1992; *Tarboton et al.*, 1991; *Montgomery and Foufoula-Georgiou*, 1993; *Giannoni et al.*, 2005; *Hancock and Evans*, 2006; *Lin et al.*, 2006]. Several criteria have been proposed for determining channel initiation from DEMs and these include a threshold on drainage area, a threshold on local slope, a combination of area and slope, and also a threshold on local curvature (e.g., see review by *Rodriguez-Iturbe and Rinaldo* [1997, chapter 1, and references therein], and *Heine et al.* [2004]). The resolution of the available DEMs and also the noise in the elevation data can considerably influence the accuracy, and thus interpretation, of the numerically computed local gradients and curvatures. In fact, "local" gradients and curvatures from typical 90 m or 30 m DEMs represent anything but local properties and in most landscapes these scales are already too large to be useful in detecting channel initiation [e.g., *Montgomery and Foufoula-Georgiou*, 1993]. It is also expected that the resolution-dependent estimates of local gradients which are drivers of geomorphic transport laws [e.g., see *Dietrich et al.*, 2003] might result in resolution-dependent sediment fluxes (e.g., see *Stark and Stark* [2001] and a recent study by *Passalacqua et al.* [2006]).

[3] High resolution (1 to 3 m data spacing) elevation data derived from airborne laser swath mapping (ALSM) now offer the opportunity to use direct topographic "signatures" of river incision and channel banks to map directly the channel network. In the uplands of tectonically active areas, the channel banks in steep small tributaries are typically cut against bedrock and lack sharp topographic boundaries relative to the hillslope. In this case, the primary topographic signature of active channel incision is the characteristic "V" shaped valleys (as compared to broadly curved valley axes). These channels rarely are plotted as "blue lines" on United States Geological Survey maps and are difficult to see in aerial photographs due to vegetation, yet they border most of the hillslopes, convey much of the sediment down to low gradient larger rivers, and constitute much of the total channel network [e.g., *Stock and Dietrich*, 2003]. Here we introduce the use of wavelet analysis to locally filter elevation data and to detect thresholds in topographic curvature and slope-direction change for defining valleys and probable channelized portions of the valley. We also propose that these topographic signatures may offer new metrics for model comparison with real landscapes.

2. Computation of Local Gradients, Curvatures, and Slope-Direction Change at Multiple Scales Using Wavelets

[4] We take advantage of the well-known property of the convolution product:

$$\frac{\partial}{\partial x}(h*g) = \frac{\partial h}{\partial x}*g = h*\frac{\partial g}{\partial x} \qquad (1)$$

which implies that smoothing a function h with a kernel g and then taking derivatives (left most term) is equivalent to taking derivatives of the function and smoothing these derivatives with the kernel g (middle term) or equivalent to smoothing the function h directly with the derivative of the kernel g (right most term). It is noted that computing first and second order derivatives from 1 m or 2 m elevation data using finite differences results in considerable noise and smoothing is usually required to reduce the noise. This is typically done by either first smoothing the topography and then computing derivatives [e.g., *Roering et al.*, 1999] or computing derivatives from the original high resolution topography and then smoothing these derivatives by averaging (e.g., *Tucker et al.* [2001], see also the review paper of *Schmidt et al.* [2003]). These methods correspond

---

[1]National Center for Earth-Surface Dynamics and St. Anthony Falls Laboratory, Department of Civil Engineering, University of Minnesota, Minneapolis, Minnesota, USA.

[2]Department of Earth and Planetary Science, University of California, Berkeley, California, USA.

to the left-most and middle terms of equation (1). Here we take advantage of the third term of the above equality which naturally introduces us to using wavelets for efficient computation of local slopes and curvatures of elevation surfaces. Specifically, the first and second derivatives of elevation heights $h(x, y)$ in the x direction (similar expressions hold for the y direction) can be written as:

$$\nabla_{x,\sigma} h(x,y) = \left(h * g_{1,\sigma,x,y}^x \right)(x,y) \qquad (2)$$

$$\nabla_{x,\sigma}^2 h(x,y) = \left(h * g_{2,\sigma,x,y}^x \right)(x,y), \qquad (3)$$

where $g_{1,\sigma,x,y}^x$ and $g_{2,\sigma,x,y}^x$ are the first and second derivatives of a 2D Gaussian function of standard deviation σ and centered at location (x, y):

$$g_{0,\sigma,x,y}(u,v) = \frac{1}{2\pi\sigma^2} \exp\left[-\frac{(u-x)^2+(v-y)^2}{2\sigma^2} \right] \qquad (4)$$

The functions $g_{1,\sigma,x,y}^x$ and $g_{2,\sigma,x,y}^x$ are proper wavelets [e.g., *Mallat*, 1999] and $g_{2,\sigma,x,y}^x$ is the so-called Mexican hat wavelet popular in many geophysical applications [e.g., see *Foufoula-Georgiou and Kumar*, 1994]. Thus the gradients and curvatures defined by equations (2) and (3) are simply (apart from a normalization) the 2D continuous wavelet transforms (CWT) of the function $h(x, y)$ with two different wavelets. Defining the "scale" associated to a wavelet as the inverse of its band-pass frequency [e.g., *Mallat*, 1999; *Kumar and Foufoula-Georgiou*, 1997] it can be shown that the smoothing scale corresponding to $g_{1,\sigma,x,y}^x$ (gradients) is $a = \pi\sigma$ and to $g_{2,\sigma,x,y}^x$ (curvatures) $a = \sqrt{2}\pi\sigma$, while the scale of topography smoothing is $a = 4\sigma$, (see Table 1). For the rest of the paper, we adopt the notation of a for scale and compute the modulus of the steepest slope $m_a(x, y)$, its direction $\theta_a(x, y)$, and also the local curvature $\gamma_a(x, y)$ at scale a and at pixel (x, y) as:

$$m_a(x,y) = \sqrt{\left(\nabla h_{x,a}(x,y)\right)^2 + \left(\nabla h_{y,a}(x,y)\right)^2} \qquad (5)$$

$$\gamma_a(x,y) = \nabla_{x,a}^2 h(x,y) + \nabla_{y,a}^2 h(x,y) \qquad (6)$$

and

$$\theta_a(x,y) = \beta\pi + arctan\left(\frac{\nabla_{y,a} h(x,y)}{\nabla_{x,a} h(x,y)} \right) \qquad (7)$$

where $\beta = 0$ if, $\nabla_{x,a} h(x, y) > 0$, $\beta = 1$ if $\nabla_{x,a} h(x, y) < 0$ and $\nabla_{y,a} h(x, y) > 0$ and $\beta = -1$ if $\nabla_{x,a} h(x, y) < 0$ and $\nabla_{y,a} h(x, y) < 0$.

[5] Channel incision in uplands topography leads to hillslopes on opposite sides that typically face each other obliquely, giving rise to "V" shaped topographic contour lines. We can use this signature to delineate the axis of valleys

and the likely pathway of channels with limited floodplain area on their boundaries. We compute the derivative of the slope direction $\theta_a(x, y)$ as

$$d\theta_a = \sqrt{\left(d_x\theta_a\right)^2 + \left(d_y\theta_a\right)^2} \qquad (8)$$

where $d_x\theta_a = (\partial\theta_a/\partial x)dx$ and $d_y\theta_a = (\partial\theta_a/\partial y)dy$ are numerically estimated with finite differences. It is noted that the slope direction θ_a is defined modulo 2π and is counterclockwise oriented. θ_a ranges between $-\pi$ to $+\pi$ and takes the value 0 when the slope exactly "points to the East". So θ_a has an abrupt 2π variation when crossing the westward direction (this is not a continuous function) and the numerical derivative will exhibit a large value that is not due to a real direction change. To overcome this numerical issue, a direction θ_a' with a different zero origin ($\theta_a' = 0$ when the slope points to the North) is computed as well as its numerical derivative $d\theta_a'$. One then only needs to define the direction derivative as $\min(d\theta_a, d\theta_a')$ in order to remove the spurious large values due to shifting between $-\pi$ and π values. The quantity $\min(d\theta_a, d\theta_a')$ will be also referred to as $d\theta_a$ in the sequel.

[6] We propose here that from the wavelet-filtered elevation data we can use the probability density function (pdf) of curvature to detect a threshold below which well-defined valleys are absent. Furthermore, we suggest that a similar threshold exists in the pdf of the slope-direction change that delineates the transition from "U" shaped valleys to "V" shaped river canyons. These two analyses can be used to define valleys associated with channel incision, and, hence, the likely channel network.

3. Statistical Signatures of Geomorphic Transitions

[7] We use the ALSM data ($\sim$2.6 m average bare earth data spacing, gridded to 1 m) acquired by NCALM for the South Fork Eel River in the coastal mountains of Northern California (available at data distribution archive http://www.ncalm.org/) to explore the use of our proposed methods. The site is a 2.8 km^2 mostly forested tributary that lies just north of the Angelo Coast Range Reserve, $\sim$3 km downstream from the junction of Ten Mile Creek and the South Fork Eel River. It receives about 1900 mm of strongly seasonal rainfall. The mainstem draining the watershed is steeper than 8% and all of its tributaries are steeper than 20%. These channels border hillslopes which are commonly pockmarked with amphitheater shaped topographic steps recording the deformation of the surface associated with extensive deep-seated landsliding. Some fine-scale topographic roughness is an artifact of dense impenetrable brush the tops of which are treated as bare earth, leading to an "acne" appearance of local areas. Based on channel slope [*Stock and Dietrich*, 2003] and field observations in similar terrain in the area, the channel network is cut by a combination of river incision and debris flow scour, perhaps tied to the periodic movement and release of sediment associated with movement of the large landslides (see also

Table 1. Smoothing Scales for Elevation, Gradients, and Curvatures Associated With the Gaussian Kernel of Standard Deviation σ From Which the Wavelets g_1 and g_2 Were Derived[a]

	Elevation, $g_{0,\sigma,x,y}^{x \text{ or } y}$	Gradients, $g_{1,\sigma,x,y}^{x \text{ or } y}$	Curvature, $g_{2,\sigma,x,y}^{x \text{ or } y}$
σ	$a = 4\sigma$	$a = 2\pi\sigma$	$a = \sqrt{2}\pi\sigma$
2 m	8 m	12.6 m	8.9 m
3 m	12 m	18.9 m	13.3 m
4 m	16 m	25.1 m	17.8 m
6 m	24 m	37.7 m	26.7 m
8m	32m	50.2m	35.5m
16m	64m	100.5m	71.1m

  [a]See equations (2) to (4).

Gangodagamage et al. [2007] for a quantitative analysis of the roughness of valley morphology in the basin).

3.1. Multiscale Variability of Curvature and Interpretation

[8] The standard deviation of the probability density function (pdf) of local curvature computed for the study watershed at different scales is shown in Figure 1. An abrupt transition emerges at a scale of approximately 12 m (parameter of the analyzing wavelet is $\sigma = 3$ m; see Table 1). For scales smaller than 12 m, curvature variability rapidly increases with decreasing smoothing scale. This rapid increase in variability we attribute to the topographic roughness created by poor bare earth data in brushy areas, and to fine scale topographic complexity associated with the numerous landslide features. The progressive decrease in variability is to be expected with increasing smoothing scale, although the well defined power law was not anticipated. The slope of this relationship may prove useful in distinguishing landscapes with different degree of dissection.

3.2. Hillslope to Valley Transition

[9] Figure 2a shows the quantile-quantile plot (variable plotted against standard normal deviate of the same exceedance probability) of curvature,, γ_a for the study site analyzed at the scale $a = 26.7$ m (well above the roughness break shown in Figure 1). The deviation from a straight line indicates a deviation of the pdf from Gaussian. The positive γ_a's (relevant to channels) deviation from a normal pdf occurs at a standard normal quantile value z of approximately 1, and a curvature of about 0.02 m^2/m. Analysis at smoothing levels from $a = 17.8$ m to $a = 71.1$ m found the value of $z \simeq 1$ to be robust and scale-independent while, of course, the specific values of γ_a at which the transition occurs will depend on scale. This implies that the threshold value of γ_a at which a change in the shape of the pdf occurs is

$$\gamma_{a,th} = F_a^{-1}(0.84) \qquad (9)$$

corresponding to $F_a(\gamma_{a,th}) = \Phi\,(z = 1) = 0.84$, where Φ is the cumulative distribution of a standard normal deviate $z \sim N(0, 1)$ and F_a is the cumulative distribution of γ_a.

[10] We suggest that the deviation from the normal distribution records an approximate break in which higher curvature values delineate well organized valley axes and lower (but still positive) values record the disordered occurrence of localized convergent topography. Figure 2c shows the areas of high curvature for the threshold value of

the standard normal deviate (z) equal to 1. Lower values of z (and thus lower curvature) greatly increased the number of isolated patches. The network in this catchment is partly disrupted by deep-seated landsliding, and this contributes to the residual patchiness and discontinuous delineation of valleys with this threshold. This multiscaling analysis suggests that rather than expecting the hillslope-valley transition to be defined by the change in sign in curvature instead, some disorganized and perhaps nascent valleys not integrated with the watershed valley network are scattered across the hillslopes and a curvature threshold extracted from an abrupt transition in the statistical distribution of curvature better defines the valley system. Analysis at smoothing levels from a = 17.8m to a = 71.1m finds this threshold to be determined by a scale-independent parameter.

3.3. Valley to Channel Transition

[11] Figure 2b shows the quantile-quantile plot of the log of the change in slope direction, for the study site analyzed at the scale a = 25.1m (comparable to the 26.7 m smoothing scale reported for curvatures in Figure 2a; see Table 1). The deviation from normality occurs at the normal quantile $z_{\log_{d\theta a}} \simeq 1.5$. As in the curvature case (Figure 2a) we propose that the break from normality (thicker than Gaussian tail) is a topographic signature of process dominance change. In this case, we suggest that this break defines the transition from broadly curved, unincised valleys (often found to contain thick colluvial deposits) and valleys with active channel incision and sediment removal. This suggests that a value

$$d\theta_{a,th} = exp^{F_a^{-1}(0.93)} \qquad (10)$$

corresponding to $F_a(\log d\theta_{a,th}) = \Phi(z = 1.5) = 0.93$ could be indicative of valleys with active channels.

[12] Figure 2d shows the grid cells that lie above the slope-direction change threshold. As can be seen, the grid cells that satisfy this criterion define a more narrow skeleton mostly within the valleys of Figure 2c although there are also fewer continuous path lines compared to Figure 2c, possibly separating channeled from unchanneled valleys.
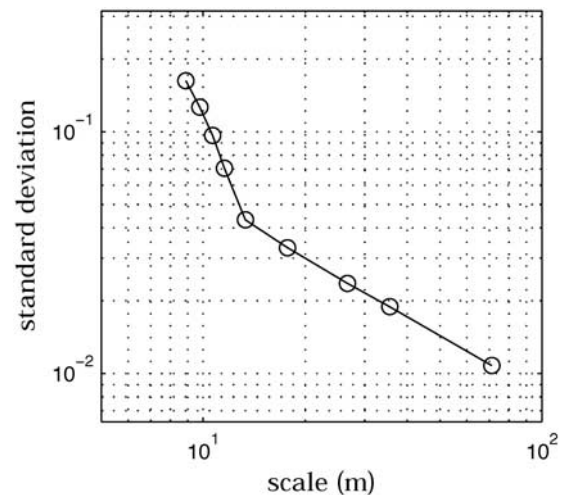

Figure 1. Scaling of the standard deviation of γ_a. The slope computed between the scales 13.3 m and 71.1 m is −0.82.
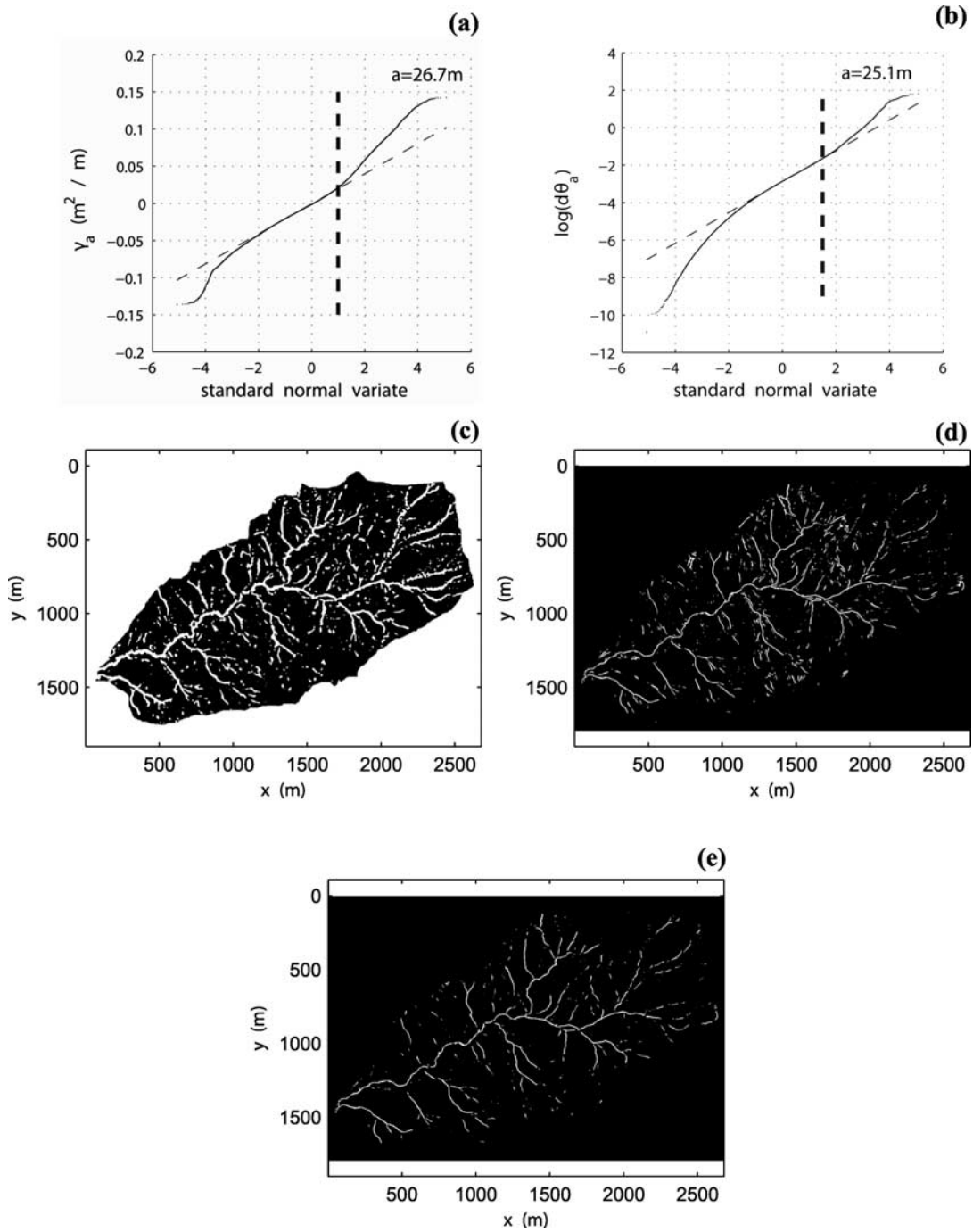
Figure 2. (a) Quantile-Quantile plot of local curvature γ_a defining the threshold curvature $\gamma_{a,th} \simeq 0.025$ for standard normal quantile z = 1. (b) Quantile-Quantile plot of $\log(d\theta_a)$, where $d\theta_a$ is the change in slope direction defining the threshold $d\theta_{a,th}$ for standard normal quantile z = 1.5. (c) The set of pixels S_1 for which $\gamma_a \geq \gamma_{a,th}$. (d) The set of pixels S_2 for which $d\theta_a \geq d\theta_{a,th}$. (e) The set of pixels that satisfy both constraints $S_1 \cap S_2$. The scale of analysis for curvatures is $a = 26.7$ m and for gradients $a = 25.1$ m (see Table 1).

By considering grid cells that satisfy both criteria of curvature and slope-direction-change threshold, a more continuous skeleton is obtained (see Figure 2e) indicating all cells most likely to be channelized.

3.4. Generating the Channel Network

[13] Starting from the likely channelized set of grids in Figure 2e, a fully connected channel network is obtained by an algorithm that connects the grid cells at which the derivative of the slope $\theta_a(x, y)$ is locally maximal. The procedure starts at the outlet and proceeds upstream linking all the $d\theta_a$ maxima along the mainstem. The extraction algorithm ends when either the derivative of the slope direction $d\theta_a$ or the curvature γ_a exceeds the thresholds $d\theta_{a,th}$ and $\gamma_{a,th}$ chosen according the statistics of $\log d\theta_a$ and γ_a (equations 9 and 10). A few other constraints were found necessary to avoid loops (which in some cases required manual intervention). The procedure is repeated for each
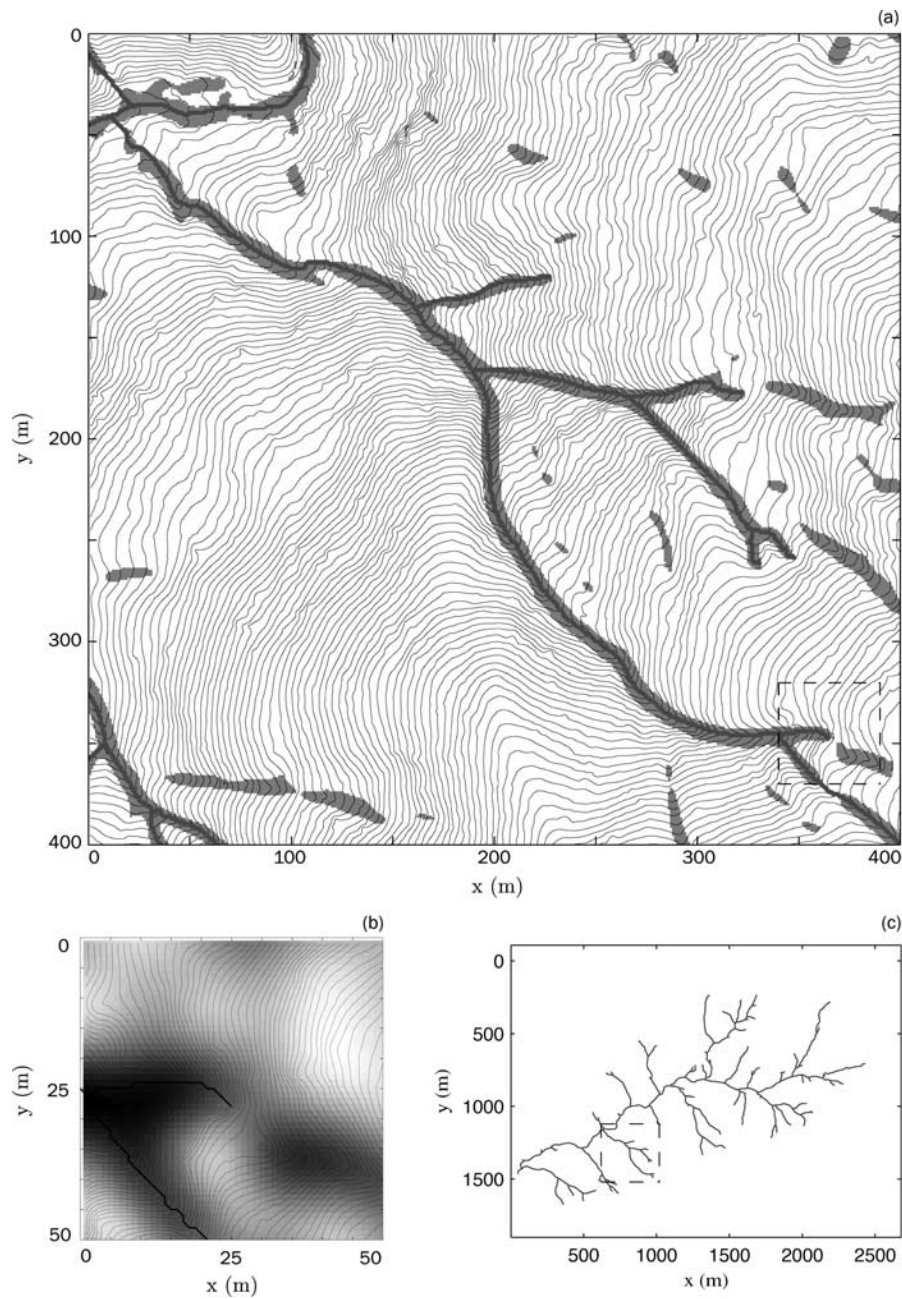
Figure 3. (a) A 400 m by 400 m area (see insert in Figure 3c) which through shading shows the set of pixels for which $\gamma_a \geq \gamma_{a,th}$ and $d\theta_a \geq d\theta_{a,th}$, and thus likely to be channelized, embedded in 2 m elevation contours. (b) A 50 m by 50 m box (see insert box in Figure 3a) showing in detail the extracted continuous channel network by tracing the centerline of the likely channelized areas shown in Figure 3a. Notice the disruption of the channel by a landslide which would be hard to identify with common methods of channel network extraction. The shading corresponds to curvature magnitude and 1m elevation contours are superimposed. (c) The continuous river network extracted for the whole river basin using the proposed methodology.

tributary junction. Junctions themselves often failed to meet one of the two criteria. However, we have resolved this issue by choosing the first point resolvable by the two thresholds and then by projecting towards the stream following the steepest gradient.

[14] The extracted river network for the study watershed is shown in Figure 3c. The insert box in Figure 3c (400 m by 400 m) is shown in detail in Figure 3a. The shaded areas in that Figure 3a are the grid cells that satisfy both threshold criteria (curvature and slope-direction-change) and thus are likely to be channelized. Note that the shaded area as it extends up into steep slopes is estimated to be highly discontinuous by this procedure. Many of the discontinuous patches are associated with the deep-seated landslide-induced steps in the topography. There is a complex interplay between landsliding and channel incision [e.g., *Kelsey*, 1978] that leaves channel traces in the topography well after movement has ceased. A smaller insert boxes (50 m by

50 m) is marked at the bottom right corner of Figure 3a, and is shown in detail in Figure 3b. In Figure 3b, the shading corresponds to curvature magnitude (darker shading for higher positive curvature) and the continuous river center-line as extracted by the proposed procedure is also shown. Figure 3b shows in detail the step-like topography associated with deep-seated landsliding and the disrupted channel network it creates. The channel head occurs on the face of a rotational block where the slope is only weakly convergent. A network drawn using just an area threshold would not have identified these discontinuities, and a method based on area and slope would generally infer incision where slopes are steep, but in the case shown in Figure 3b it would have incorrectly extended an inferred channel across topography that lacks the convergence and slope-change signature of channel incision. Hence, we propose that our procedure provides a more realistic, topographically-driven delineation of the likely channeled portions of the landscape.

4. Conclusions

[15] We proposed a wavelet-based filtering procedure that allows us to compute local curvature and slope-direction-change across scales and exploit their statistical structure for inferring physical transitions. Specifically, deviation of the positive tails of the pdfs of curvature and slope-direction-change from normality and log-normality, respectively, revealed two threshold values corresponding to approximately scale-invariant quantiles (16% exceedance quantile for curvatures and 7% for slope-direction-change). We interpret these breaks in the pdfs as arising from topographic signatures of process change and use the emerging threshold values to delineate valleys (from the curvature threshold) and channelized parts within those valleys (from the slope-direction-change threshold). We report a power law relationship of curvature variance with scale with a major break at a characteristic scale (of approximately 12 m) and two distinct scaling regimes: one at small scales reflecting roughness changes due to vegetation (and other) effects, and one at larger scales due to a progressive smoothing of the landscape variability by coarse graining. These new multiscale statistical relationships and the identified thresholds have been used to propose a methodology for objective extraction of channel networks in canyon upland rivers from high resolution LIDAR topography. They also offer new metrics which might be useful in refining and testing landscape evolution theories and in upscaling geomorphic transport laws.

References

Costa-Gabral, M. C., and S. J. Burges (1994), Digital elevation model networks (DEMON): A model flow over hillslopes for computation of contributing and dispersal areas, *Water Resour. Res.*, 30, 1681–1692.

Dietrich, W. E., D. Bellugi, A. M. Heimsath, J. J. Roering, L. Sklar, and J. D. Stock (2003), Geomorphic transport laws for predicting the form and evolution of landscapes, in *Prediction in Geomorphology*, Geophys. Monogr. Ser., vol. 135, edited by P. Wilcock and R. Iverson, pp. 103–132, AGU, Washington, D. C.

Foufoula-Georgiou, E., and P. Kumar (Eds.) (1994), *Wavelets in Geophysics*, 372 pp., Academic, New York.

Gangodagamage, C., E. Barnes, and E. Foufoula-Georgiou (2007), Scaling in river corridor widths depicts organization in valley morphology, *Geomorphology*, 91, 198–215.

Giannoni, F., G. Roth, and R. Rudari (2005), A procedure for drainage network identification from geomorphology and its application to the prediction of the hydrologic response, *Adv. Water Res.*, 28, 567–581.

Hancock, G. R., and K. G. Evans (2006), Channel head location and characteristics using digital elevation models, *Earth Surf. Processes Landform*, 31, 809–826.

Heine, R. A., C. L. Lant, and R. R. Sengupta (2004), Development and comparison of approaches for automated mapping of stream channel networks, *Ann. Assoc. Am. Geogr.*, 94(3), 477–490.

Kelsey, H. M. (1978), Earthflows in Franciscan melange, Van Duzen River basin, California, *Geology*, 6, 361–365.

Kumar, P., and E. Foufoula-Georgiou (1997), Wavelet analysis for geophysical applications, *Rev. Geophys.*, 35(4), 385–412.

Lin, W., W. Chou, C. Lin, P. Huang, and J. Tsai (2006), Automated suitable drainage network extraction from digital elevation models in Taiwan's upstream watersheds, *Hydrol. Processes*, 20, 289–306.

Mallat, S. (1999), *A Wavelet Tour of Signal Processing*, 2nd ed., Academic, San Diego, Calif.

Montgomery, D. R., and W. E. Dietrich (1988), Where do channels begin?, *Nature*, 336, 232–234.

Montgomery, D. R., and W. E. Dietrich (1989), Source areas, drainage density and channel initiation, *Water Resour. Res.*, 25, 1907–1918.

Montgomery, D. R., and W. E. Dietrich (1992), Channel initiation and the problem of landscape scale, *Science*, 255, 826–830.

Montgomery, D. R., and E. Foufoula-Georgiou (1993), Channel network source representation using digital elevation models, *Water Resour. Res.*, 29, 3925–3934.

Passalacqua, P., F. Porté-Agel, E. Foufoula-Georgiou, and C. Paola (2006), Application of dynamic subgrid-scale concepts from large-eddy simulation to modeling landscape evolution, *Water Resour. Res.*, 42, W06D11, doi:10.1029/2006WR004879.

Rodriguez-Iturbe, I., and A. Rinaldo (1997), *Fractal River Basins: Chance and Self-Organization*, Cambridge Univ. Press, New York.

Roering, J., J. Kirchner, and W. E. Dietrich (1999), Evidence for nonlinear, diffusive sediment transport on hillslopes and implications for landscape morphology, *Water Resour. Res.*, 35(3), 853–870.

Schmidt, J., I. S. Evans, and J. Brinkmann (2003), Comparison of polynomial models for land surface curvature calculation, *Int. J. Geogr. Inf. Sci.*, 17(8), 797–814.

Stark, C. P., and G. J. Stark (2001), A channelization model of landscape evolution, *Am. J. Sci.*, 301, 486–512.

Stock, J., and W. E. Dietrich (2003), Valley incision by debris flows: Evidence of a topographic signature, *Water Resour. Res.*, 39(4), 1089, doi:10.1029/2001WR001057.

Tarboton, D. R. (1997), A new method for the determination of flow directions and contributing areas in grid digital elevation models, *Water Resour. Res.*, 33, 309–319.

Tarboton, D. R., R. L. Bras, and I. Rodriguez-Iturbe (1991), On the extraction of channel networks from digital elevation data, *Hydrol. Processes*, 5, 81–100.

Tucker, G. E., F. Catani, R. L. Bras, and A. Rinaldo (2001), Statistical analysis of drainage density from digital terrain data, *Geomorphology*, 36, 187–202.

————————————
W. E. Dietrich, Department of Earth and Planetary Science, University of California, Berkeley, McCone Hall, Berkeley, CA 94720, USA.

E. Foufoula-Georgiou and B. Lashermes, National Center for Earth-Surface Dynamics and St. Anthony Falls Laboratory, Department of Civil Engineering, University of Minnesota, 382 SAFL, 2 34th Avenue SE, Minneapolis, MN 55414, USA. (efi@umn.edu)